Phase separation analysis of bulk heterojunctions in small-molecule organic solar cells using zinc-phthalocyanine and C_{60}

Christoph Schünemann,[1,*] David Wynands,[2,†] Lutz Wilde,[3] Moritz Philipp Hein,[1] Steffen Pfützner,[1,‡] Chris Elschner,[1] Klaus-Jochen Eichhorn,[2] Karl Leo,[1,§] and Moritz Riede[1]

[1]*Institut für Angewandte Photophysik, Technische Universität Dresden, D-01069 Dresden, Germany*

[2]*Leibniz-Institut für Polymerforschung Dresden e.V., D-01005 Dresden, Germany*

[3]*Fraunhofer Center Nanoelectronic Technologies (CNT), 01099 Dresden, Germany*

(Received 12 April 2012; published 21 June 2012)

To achieve efficient organic solar cells, donor and acceptor molecules are mixed in the photoactive layer to form a so-called bulk heterojunction. Due to molecular interactions, a certain degree of phase separation between donor and acceptor domains arises, which is necessary to achieve efficient charge extraction within the absorber layer. However, the mechanism that induces the phase separation is not fully understood and gaining detailed information about the molecular arrangement within these blend layers is quite challenging. We show that grazing incidence x-ray diffraction, combined with variable angle spectroscopic ellipsometry is a suitable way to investigate the molecular structure of blend layers in detail, consisting of a mixture of zinc-phthalocyanine (ZnPc) and C_{60}. The degree of phase separation within the blend layer is influenced by substrate heating during the co-evaporation of ZnPc and C_{60} and by a variation of the mixing ratio. The effect of different blend layer morphologies on optical and electrical device performance is investigated by solar cell characterization and mobility measurements. We find that the molecular arrangement of C_{60} provides the essential driving force for efficient phase separation. Whereas spherical C_{60} molecules are able to form crystalline domains when deposited at elevated substrate temperatures, no ZnPc crystallites are observed, although the planar ZnPc molecules are not randomly oriented but standing upright within its domains. Comparing specular and grazing incidence x-ray diffraction, we find that only the latter method is able to detect nanocrystalline C_{60} in thin films due to its polycrystalline nature and small sized nanocrystallites. Solar cell measurements show an increase in fill factor and external quantum efficiency signal for blends with enhanced phase separation, induced by higher substrate temperatures. However, grazing incidence x-ray diffraction measurements reveal that ZnPc and C_{60} already form separate domains in unheated ZnPc:C_{60} blends, which provide fill factors close to 50% in the corresponding solar cells.

DOI: 10.1103/PhysRevB.85.245314 PACS number(s): 64.75.Qr, 78.40.Me, 88.40.jr, 79.60.Jv

I. INTRODUCTION

In the last decade, organic solar cells have achieved impressive progress. Both polymer and small molecule organic solar cells reach power conversion efficiencies approaching 10%.[1]The major challenge to achieve further improvements originates in the high binding energy of several 100 meV of the excitons created by absorption within the organic photoactive layer.[2] So the instantaneous dissociation of the Frenkel excitons into free charges is highly unlikely. However, exciton separation is very efficient at interfaces of organic acceptor and donor molecules.[3] One way to achieve a donor-acceptor interface is to deposit two planar layers consecutively: one containing the donor and the other the acceptor material. This kind of photoactive layer is called planar heterojunction (PHJ).[3] On the one hand, the photoactive layer thickness of PHJ solar cells is limited, since exciton diffusion length is in the range of only 10 nm for most organic materials.[4] On the other hand, the light penetration depth is much larger (in the order of 100 nm), thus such thin photoactive layers consequently absorb only fewer photons and thus the photocurrent is limited for PHJ's.[5,6] A possibility to overcome this problem is mixing of donor and acceptor molecules to form a so-called bulk heterojunction (BHJ).[7–9] In blend layers, the interface between donor and acceptor is strongly increased which leads to an improvement of exciton separation and allows to use thicker absorber layers, harvesting more sunlight. On the one hand, the challenge is to guarantee closed percolation paths for photogenerated electrons and holes towards the electrodes.[10] Hence the formation of isolated donor or acceptor domains should be avoided within blend layers. On the other hand, phase separation should not result in domains larger than the exciton diffusion length to achieve efficient exciton dissociation. Otherwise, the same problem as for the planar heterojunction occurs. Thus it is essential to find the optimized kind of phase separation of donor and acceptor, i.e., the optimized blend morphology. One possibility to achieve insights into the phase separation mechanism is their modeling using the Ising model and Monte Carlo simulations. These results show an increase of phase separation and donor/acceptor domain sizes for elevated temperatures, i.e., higher kinetic energies of the molecules.[11–13] Experimental evidences for phase separation are mainly carried out using electron or atomic force microscopy, x-ray diffraction, and absorption measurements.[14–16]

A common approach to influence the phase separation in small molecular BHJ organic solar cells is the use of substrate heating during deposition of the blend layer in vacuum as well as changing the mixing ratio of donor and acceptor.[17–19] For polymer BHJ solar cells, postannealing of the blend layer is the most common way to obtain enhanced morphology.[16,20] However, to understand the complex growth mechanism of blend layers and gaining detailed experimental information about their morphology is quite challenging and only a few experimental methods are suitable for this.

TABLE I. Overview about the ZnPc:C_{60} blend layers prepared for a direct comparison of the morphology (GIXRD, AFM, ellipsometry) and electro-optical characterization (solar cells and mobility measurements). The blend layers are deposited on a glass substrate coated with 5-nm C_{60} for GIXRD and AFM measurements and directly on glass for absorption measurements (*1). Within fabricated solar cells, the ZnPc:C_{60} layers are evaporated on ITO substrate/5-nm *n*-doped C_{60}/20-nm C_{60} (*2). For ellipsometry measurements, the blend layers are deposited on Interference Enhanced Substrates (SiO_2) (*3) and for mobility measurements on SiO_2 substrate with patterned gold contact (*4).

Blend layer structure	GIXRD, AFM, absorption (*1)	Solar cells (*2)	Ellipsometry (*3)	Mobility (*4)
ZnPc:C_{60} 1:1, $T_{sub} = 30\,^{\circ}C$	150-nm thick	60-nm thick	100-nm thick	40-nm thick
ZnPc:C_{60} 1:1, $T_{sub} = 100\,^{\circ}C$	150-nm thick	60-nm thick	100-nm thick	40-nm thick
ZnPc:C_{60} 1:1, $T_{sub} = 140\,^{\circ}C$	150-nm thick	60-nm thick	–	40-nm thick
ZnPc:C_{60} 1:2, $T_{sub} = 140\,^{\circ}C$	150-nm thick	60-nm thick	–	–
ZnPc:C_{60} 2:1, $T_{sub} = 140\,^{\circ}C$	150-nm thick	60-nm thick	–	–

In this study, we investigate the influence of substrate heating and different blend ratios of zinc-phthalocyanine (ZnPc) and C_{60} small molecules in blend layers on the morphology and directly relate these findings with solar cell and organic field effect transistor (OFET) performances. The blends are analyzed by grazing incidence x-ray diffraction (GIXRD), atomic force microscopy (AFM), and variable angle spectroscopic ellipsometry (VASE). GIXRD measurements reveal detailed information about the molecular arrangement within the layer and depict the central method to achieve information about ZnPc and C_{60} arrangement within the blend layers.[21,22] VASE enables a more detailed characterization of the molecular orientation of ZnPc in the blend by measuring the anisotropic optical constants.[23,24] AFM images are taken to complete the investigations of phase separation. Finally, the influence of the different blend morphologies on solar cell and OFET performance are discussed.

For all investigations, we used blend layers with comparable morphologies by depositing the film using the same parameters. In Table I, all samples are presented. We vary the blend ratio of ZnPc:C60 (2:1, 1:1, 1:2 vol%) and the substrate temperature ($T_{sub} = 30$, 100, and 140 ;°C) in the same manner for all morphology measurements and solar cells applications. Only the kinds of substrate and layer thickness are different to some extent. The blend layer morphology is found to be independent on the substrates and on the layer thickness we use in this study, figured out by GIXRD and AFM measurements. To achieve high comparability of all solar cells and morphological samples, we process all solar cells and morphological samples within one run, respectively.

II. EXPERIMENTAL

The materials are thermally evaporated at a base pressure of 10^{-7},...,10^{-8} mbar. Within the solar cells N,N'-((Diphenyl-N,N'-bis)9,9,-dimethyl-fluoren-2-yl)-benzidine (BF-DPB) doped with 10 wt% 2,2'-(perfluoronaphthalene-2,6-diylidene)dimalononitrile (F6-TCNNQ, Novaled AG, Dresden, Germany) is used as *p*-doped hole transport layer and C_{60} doped with 2 wt% tetrakis(1,3,4,6,7,8-hexahydro-2H-pyrimido[1,2]-apyrimidinato)ditungsten (II) [W2(hpp)4, Novaled AG, Dresden, Germany] as *n*-doped electron transport layer.[38] ZnPc (TCI Europe, Germany), C_{60} (IPMS, Dresden, Germany), and BF-DPB (Sensient) are purified at least twice by vacuum gradient sublimation before thin film preparation. All solar cells are deposited onto indium tin oxide coated glass substrates [Thin Film Devices, USA (sheet resistance <30 Ω/sq)] pretreated with organic solvents in an ultrasonic bath and by oxygen plasma cleaning. For the organic materials, we use the following thin film densities, determined by profilometer measurements: $\rho_{ZnPc} = 1.34\ g/cm^3$, $\rho_{C60} = 1.54\ g/cm^3$, $\rho_{BF-DPB} = 1.04\ g/cm^3$.

Pristine films of ZnPc and C_{60} as well as ZnPc:C_{60} blend layers for mobility and ellipsometry measurements are deposited via thermal evaporation in a multichamber UHV system (Bestec, Germany). Blend layers of ZnPc:C_{60} are prepared by coevaporating ZnPc and C_{60} from two crucibles using deposition rates of 0.3Å/s for ZnPc and C_{60} for blend ratio of 1:1 and 0.2Å/s for ZnPc and 0.4Å/s for C_{60} for a blend ratio of 1:2 and vice versa for 2:1 by volume. Quartz crystal microbalances are used to control the layer thickness. 150-nm ZnPc:C_{60} blend films, used for morphological investigations, as well as solar cell devices are fabricated in a custom-made single chamber vacuum system (K. J. Lesker, UK). It offers the opportunity to produce 36 different samples within one process. Each of the samples consists of four solar cells with identical device stacks to ensure the reproducibility. All pristine and blend films for morphological investigations cover an area of 20 mm × 20 mm on the substrate to ensure a high-scattering area of the thin layer for x-ray diffraction investigations.

The solar cells are encapsulated in a nitrogen glovebox prior exposure to ambient conditions and characterized using a 16 S-003-300 sun simulator (Solarlight Company Inc., USA) and a Keithley Source Measure Unit (SMU2400). For all devices, we use the same nominal illumination intensity I_{nom} of 128 mW/cm^2 as measured by a calibrated silicon reference diode (Fraunhofer ISE, Freiburg, Germany). Spectral response or external quantum efficiency is measured with a lock-in amplifier (Signal Recovery SR7265) with the phase set to the frequency of the mechanical chopper used to chop the incident light. A Xe lamp coupled with a monochromator (Newport Oriel Apex) is used as light source. The intensity of the incident light is measured at each wavelength with a calibrated Si photodiode (Hamamatsu). The mismatch corrected power conversion efficiency is calculated using an effective intensity I_{eff} that corresponds to the product of I_{nom} and the mismatch factor determined from the EQE measurements of the solar cells.

Out-of-plane grazing incidence (GIXRD) and specular (Bragg-Brentano geometry) x-ray diffraction measurements are performed using a Bruker D8 Discover diffractometer at the Fraunhofer CNT (Dresden, Germany). The CuKα1

radiation beam positioned through a Göbel mirror on the thin film sample and the resulting scattered signals are recorded by a scintillation detector. The incident x-ray beam is kept fixed at $2\theta = 0.20^\circ$ and only the detector angle is varied in 2θ steps of 0.1° (recording time per angle step: 30 seconds) for GIXRD measurements. The specular ω-2θ scan mode was only used for a 50-nm thick C_{60} layer, all other measurements are performed by the GIXRD scan mode. Details about the GIXRD measurement routine is described by Elschner *et al.*[22] All x-ray patterns are not background corrected. The topography and the root-mean-square (RMS) roughness of the ZnPc:C_{60} blend layers is investigated using a Combiscope 1000 (AIST NT) in the intermittent contact mode with a tip amplitude of 100 nm and a spring constant of 40 N/m at ambient conditions. Absorption measurements of the ZnPc:C_{60} blend layers are determined from reflection and transmission measurement using a Lambda 900 transmission spectrometer (Perkin-Elmer).

Bottom-gate organic field effect transistors with a *p*-Si/SiO_2 gate and predeposited gold contacts with channel lengths between 5 and 20 μm (IPMS, Dresden, Germany) are used to estimate the electron and hole mobility from the saturation regime of the OFET characteristics. Further details can be found in Ref. 30.

The uniaxial anisotropic optical constants of the sample are measured by VASE. This ellipsometric method measures the polarization change of the reflected light for different incident angles. A detailed discussion of ellipsometry can be found in several textbook references.[39,40] In order to derive precise results, we use interference enhanced substrates, i.e., silicon wafer with an additional 970-nm thick layer of SiO_2.[24,41] These substrates are cleaned using sonication in aqueous detergent, acetone, ethanol, and finally isopropanol. VASE measurements are done at an M2000 UI ellipsometer (J. A. Woollam Co., Inc.), covering the wavelength range of 245 to 1680 nm. The incident angles are varied from 55° to 75° in 5° steps. Analysis of the measured data was performed using the WVASE32 software from J. A. Woollam Co., Inc. which benefits from the Levenberg-Marquardt algorithm for fitting. To reach results, that fulfill Kramers-Kronig consistency, we used the harmonic oscillator approach applying several Gaussian oscillators,[39] Details of the evaluation procedure are described in Ref. 24.

The uniaxial anisotropic samples exhibit birefringence as well as different extinction coefficients of the in-plane and out-of-plane components. From the corresponding peak positions of the extinction coefficients we evaluate the ratio $k_{\mathrm{in-plane}}/k_{\mathrm{out-of-plane}}$ and the orientation order parameter

$$S = P_2(\cos\theta) = \frac{1}{2}\langle 3\cos^2\theta - 1\rangle = \frac{k_{\mathrm{out-of-plane}} - k_{\mathrm{in-plane}}}{k_{\mathrm{out-of-plane}} + 2k_{\mathrm{in-plane}}},$$

where θ is the angle between the molecular transition dipole and the direction perpendicular to the substrate surface, $\langle\cdots\rangle$ is the ensemble average and $P_2(x)$ is the second Legendre polynomial.[23] $S = -0.5$ denotes an orientation of the molecular transition dipole ordered perfectly parallel to the substrate, while $S = 1$ denotes a perfect perpendicular orientation. $S = 0$ when there is either no order, i.e., random orientation, or all transition dipoles being perfectly oriented in a 54.7° angle.

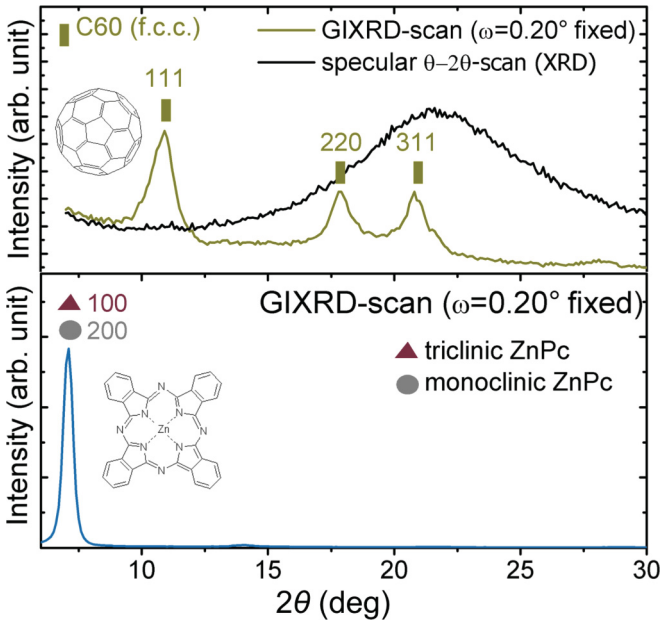

FIG. 1. (Color online) (Top) Specular XRD scan (symmetric θ-2θ-scan mode) in Bragg-Brentano geometry (black line) and out-of-plane GIXRD scan ($\omega = 0.20^\circ$ fixed, green/bright line) of a 50-nm thick pristine C_{60} layer deposited on unheated glass substrate. (Bottom) Out-of-plane GIXRD scan of a 50-nm thick pristine ZnPc layer also deposited on an unheated glass substrate (blue line).

III. RESULTS AND DISCUSSION

A. Blend layer morphology

First, we analyze the morphology of ZnPc:C_{60} blend layers deposited on heated and unheated substrates for different blend ratios by out-of-plane GIXRD, AFM, VASE, and absorption measurements. In order to interpret the x-ray diffraction pattern of ZnPc:C_{60} blend layers, we characterize a 50-nm thick pristine C_{60} and 50-nm thick ZnPc layer deposited on an unheated glass substrate using GIXRD. The x-ray pattern of the ZnPc layer in Fig. 1 reveals a 100 or 200 ZnPc Bragg reflection and higher orders of triclinic α-ZnPc or monoclinic γ-ZnPc, which is often reported in literature for ZnPc thin films.[21] We are not able to distinguish between monoclinic and triclinic phases because both show a Bragg reflection at 2θ of around 7°. Considering the observation of this reflection at low 2θ angles implies, that the ZnPc molecules in this crystallites are oriented standing upright with respect to the substrate surface for both crystallographic phases.[21] However, with out-of-plane GIXRD we can only scan a fraction of the reciprocal space and amorphous film regions are also not detected. Hence, this upright standing orientation is only valid for crystallites causing the 2θ reflection at 7°. The GIXRD pattern of C_{60} in Fig. 1 shows three distinct Bragg reflections which are attributed to the face-centred-cubic phase of C_{60} with $a = 14.224$ Å, as described by Elschner *et al.*[22] Accordingly, both ZnPc and C_{60} are able to crystallize in pristine layers. To illustrate the importance of the GIXRD measurement method we also record a specular x-ray diffraction (XRD) scan (Bragg-Brentano geometry) of the same C_{60} sample using the same x-ray tool. The XRD pattern (black line in Fig. 1) reveals that the C_{60} film is amorphous because no Bragg reflections

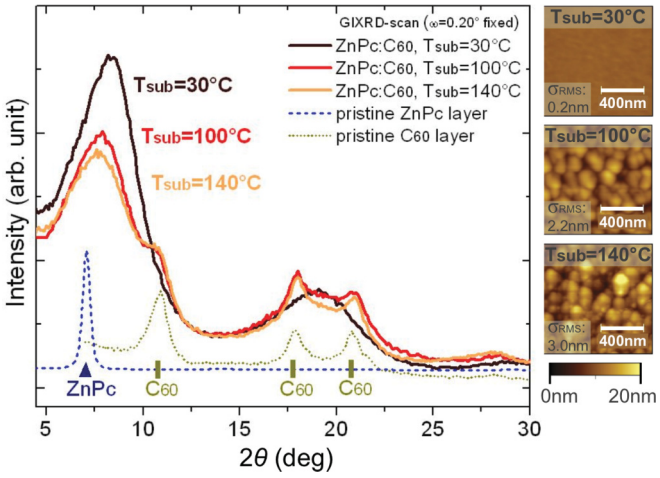

FIG. 2. (Color online) GIXRD pattern of 150-nm thick ZnPc:C_{60} (1:1) blend layers deposited at different substrate temperatures on glass/5-nm C_{60} with the corresponding AFM micrographs and resulting AFM roughness. The GIXRD pattern of a 50-nm thick pristine ZnPc and of a 50-nm thick pristine C_{60} layer is inserted to correlate the Bragg reflections of the ZnPc:C_{60} blend layers.

are visible, apart from a broad peak originated from the glass substrate. In the GIXRD scan mode, the incident angle ω of the x-ray beam is fixed at 0.20° and only the detector angle 2θ is varied. Therefore the x-ray beam only penetrates the C_{60} layer but not the glass substrate, because of the total reflection at the glass-C_{60} interface for such a small angle of incidence.[22] Consequently, the scattering in C_{60} is strongly enhanced which leads to an increased signal and the observation of three distinct Bragg reflections of C_{60} using this scan mode. For preferentially oriented organic molecules within thin films, like ZnPc, the Bragg reflections are intense enough to be detected by specular XRD scan mode. However, the GIXRD scan mode is indispensable when measuring polycrystalline or nanocrystalline films, like C_{60}.

Most x-ray measurements on blend layers including C_{60} are only done in specular XRD scan mode.[14,25,26] Using this method, these studies did not observe any Bragg reflection of C_{60} and hence argued that C_{60} grows amorphous, even for pristine C_{60} layers.[25] Considering our finding C_{60} rather seems to be growing nanocrystalline and not amorphous, because specular XRD is not able to detect this in such thin layers.

In consequence, all x-ray diffraction measurements of ZnPc:C_{60} blend layers are performed in out-of-plane GIXRD scan mode. In Fig. 2, the x-ray pattern of 150-nm-thick ZnPc:C_{60} (1:1 vol.%) blend layers deposited for substrate temperatures (Tsub) of 30, 100, and 140 °C on 5-nm C_{60}/glass are presented. Two broad peaks are visible for the unheated blend layer. Comparing this pattern with the observed reflections of ZnPc and C_{60} in the pristine layers (see Fig. 1) we are able to identify the two broad peaks of the unheated ZnPc:C_{60} blend. The first peak at $2\theta = 8°$ is caused by the overlap of ZnPc and a minor part of C_{60}, whereas the second one at $2\theta = 18°$ originates from C_{60}. The full width half maximum (FWHM) of the Bragg reflections reveals information about the quality of the molecular arrangement, i.e., crystallite size and microscopic strain.[21] On the one hand, the large FWHM of both peaks indicates a very small crystallite size and/or a very high microscopic stress/strain for ZnPc and C_{60}. On the other hand, the observation of these two distinct peaks directly implies that ZnPc and C_{60} are phase separated even for unheated blend layers. If ZnPc and C_{60} are not phase separated, no distinct peaks would be visible for ZnPc-ZnPc and C_{60}-C_{60} arrangements. The position of the ZnPc peak at $2\theta = 8°$ indicates that at least a fraction of the ZnPc molecules are not randomly oriented within their domains but at least fractionally standing upright, as in pristine ZnPc layers. However, the broad shape of the reflections points out, that the molecular arrangement of ZnPc and C_{60} is strongly disturbed when coevaporating both sort of molecules to one blend layer. In more detail, a broadening of the Bragg reflection can be caused by a decreased crystallite size or/and an increased microscopic strain within the crystallites. Hence it is correlated to a more disturbed formation of crystallites.

For samples with substrate temperatures of 100 or 140 °C during deposition of the blends, the GIXRD pattern in Fig. 2 change significantly. For $T_{sub} = 100$ °C the broad peak at $2\theta = 8°$ splits into the ZnPc peak and a 111 Bragg reflection of C_{60}. The peak at $2\theta = 18°$ also splits into two Bragg reflections, both belonging to C_{60} crystallites (220 and 311 orientation). The resulting FWHM of the Bragg reflections of C_{60} are much smaller than for the unheated blend layer. This indicates that C_{60} grows polycrystalline within its domains when heating the substrate. In contrast, the FWHM of ZnPc remains unchanged, denoting that ZnPc remains nanocrystalline or amorphous. Increasing the substrate temperature from 100 to 140 °C no significant enhancement in crystallinity is observed. The RMS roughness, determined by AFM measurements (see Fig. 2), of the layers increases from less than 1 nm for unheated to 3 nm for 140 °C substrate heated blends. This confirms the tendency of amorphous, smooth growth for nonsubstrate heated and crystalline, grainy growth for heated ZnPc:C_{60} layers.

The observation that C_{60} is able to crystallize but ZnPc not, indicates that the molecular stacking of C_{60} molecules to energetically or sterically minimizing crystalline arrangement is preferred in comparison to ZnPc molecules which remain nanocrystalline or amorphous. This indicates that C_{60} stacking might be the driving force for phase separation in ZnPc:C_{60} blends. Because of its spherical shape, C_{60} can arrange more easily in a dense crystalline packing compared to the planar shaped ZnPc molecule. Simon *et al.* also found C_{60} crystallites in ZnPc:C_{60} layers using transmission electron microscopy.[27]

Another striking evidence for the argumentation that C_{60} is the driving force in crystallization is the significant difference in glass transition temperature T_g. Kumar *et al.*[42] observed a T_g of 510 K for ZnPc, whereas the T_g of C_{60} is at 90 K and thus much lower.[43] Additionally, the C_{60} molecule is known to rotate in thin films at room temperature in its crystalline fcc structure.[43] This clearly high molecular mobility indicates that C_{60} seems to be more mobile than ZnPc, which is planar and thus do not show such rotation.

Besides changing the substrate temperature, the variation of the blend ratio of ZnPc:C_{60} is expected to influence the phase separation. Therefore we vary the blend ratio of ZnPc:C_{60} layers from 2:1, 1:1 up to 1:2 (vol%) deposited at $T_{sub} = 140$ °C on 5-nm C_{60}/glass. The GIXRD diffraction pattern in Fig. 3 is different for different blend ratios. The intensity of the ZnPc peak changes due to the different ZnPc content

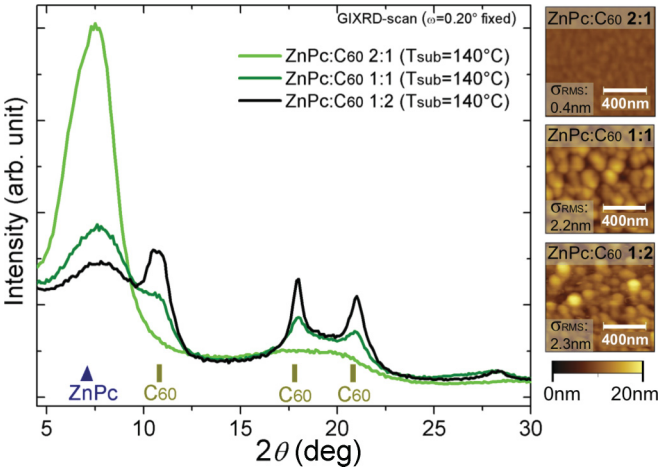

FIG. 3. (Color online) GIXRD pattern of 150-nm-thick ZnPc:C_{60} blend layers deposited at a substrate temperature of 140 °C on glass/5-nm C_{60} for different blend ratios of 2:1, 1:1, and 1:2. For the corresponding AFM micrographs and resulting AFM roughness the same samples are taken.

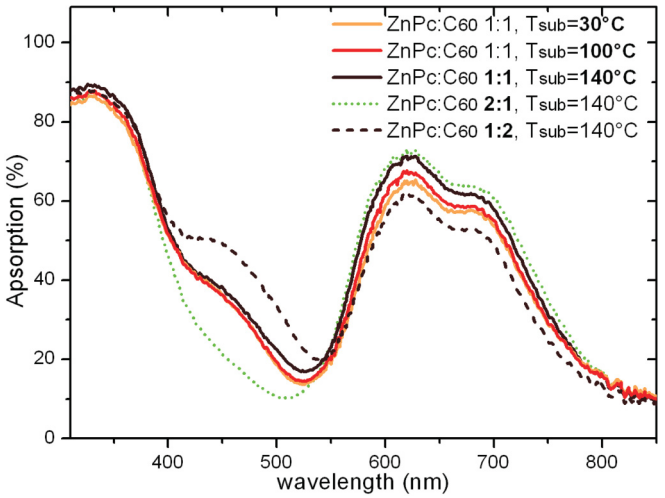

FIG. 4. (Color online) Absorption of 150-nm-thick ZnPc:C_{60} blend layers deposited on glass with varied blend ratio and substrate temperature measured via transmission and reflection measurements.

in the blend layers, but the FWHM remains almost constant. More pronounced is again the change in arrangement of the C_{60} molecules. For the heated 2:1 ZnPc:C_{60} blend, only a broad peak of C_{60} is visible, indicating that C_{60} is almost nanocrystalline or amorphous, comparable to the unheated 1:1 blend layer in Fig. 2. When changing the ratio to lower ZnPc content, C_{60} starts to crystallise in its domains and the three previously observed Bragg reflections of C_{60} occur. The AFM images confirm this trend by a low RMS roughness of less than 1 nm for the 2:1 ZnPc:C_{60} blend compared to the blends with higher C_{60} content with roughness higher than 2 nm. Combining this, ZnPc significantly disturbs the formation of C_{60} crystallites when using higher ZnPc contents, even at a high substrate temperature of 140 °C. This is again astrong evidence that C_{60} plays a major role for the phase separation, whereas ZnPc molecules are not able to form crystallites, even at high ZnPc contents and high T_{sub}.

Another possibility to prove if the ZnPc arrangement is changed within the different blends is to compare ZnPc:C_{60} absorption. Maennig *et al.* showed that the distance between the maxima within the Q-absorption bands of ZnPc and the ratio of their maxima should change for different ZnPc crystallinity.[28] However, the absorption spectra of the 150-nm thick ZnPc:C_{60} blend layers using different substrate temperatures and blend ratios in Fig. 4 show no significant difference in absorption. The absorption maxima of the Q band are constant at 625 nm and 680 nm without any change in their absorption ratio. This band arises from π-π^* transitions with the dipole moment in the plane of the molecule.[29] The detailed analysis of the thin film absorption spectra of ZnPc and C_{60} can be found elsewhere.[18] This confirms that ZnPc crystallinity is unchanged for all blend layers as found by the GIXRD measurements.

To obtain more information about the ZnPc orientation, VASE measurements are carried out for 100-nm-thick ZnPc:C_{60} (1:1) blend layers deposited on unheated and 100 °C heated SiO_2 substrates. GIXRD and AFM measurement show similar ZnPc:C_{60} growth on SiO_2 and glass/5-nm C_{60}. Hence samples for GIXRD, AFM, and VASE are comparable.

When rotating the samples around the z-axis equal measurement results are obtained, indicating that there is no in-plane anisotropy present. However, the samples turn out to be uniaxially anisotropic. In Fig. 5, the optical constants of both samples are presented. The optical model is built using 7 Gaussian oscillators, three of which are denoted to the low energy absorption of ZnPc at 600 nm to 800 nm, known as the Q band. Since C_{60} itself is isotropic, the observed anisotropy indicates preferential orientation of the ZnPc molecules.[24] In the unheated blend layer significant birefringence of $\Delta n(l = 1200\ \text{nm}) = -0.147$ is detected and the extinction coefficients in the peak of the lowest energy absorption band (684 nm) exhibit a ratio of $k_{\text{in-plane}}/k_{\text{out-of-plane}} = 0.65$, corresponding to orientation order parameter $S = 0.15$. Considering the fact that this absorption band is denoted to ZnPc while C_{60} is not absorbing at this wavelength we can deduce the ZnPc orientation from this anisotropy. The value implies that ZnPc molecules are preferentially oriented in a standing position with tilt angle of 49° of the molecular axis towards the surface normal.

When comparing the heated and unheated blend layer, the degree of anisotropy is slightly lower for the substrate heated ZnPc:C_{60} blend, showing lower birefringence of $\Delta n(l = 1200\ \text{nm}) = -0.086$ and a ratio $k_{\text{in-plane}}/k_{\text{out-of-plane}} = 0.76$ in the lowest energy absorption peak. Related to this effect, an increase of the in-plane absorption with increasing substrate temperature is observed. Correspondingly, the absorption spectra, measured at normal incidence, show higher absorption of ZnPc when higher Tsub are used (see Fig. 4). One reason for this reduction of anisotropy, i.e., lower preferential orientation, might be that the enhanced crystalline growth of C_{60} with rising substrate temperature disturbs the molecular arrangement of ZnPc in the blend layer. Using GIXRD, only the orientation of the molecules within the detected crystallites can be indicated. In contrast, VASE measurements provide the mean molecular orientation of the whole film and thus are complementary to the GIXRD measurement results.

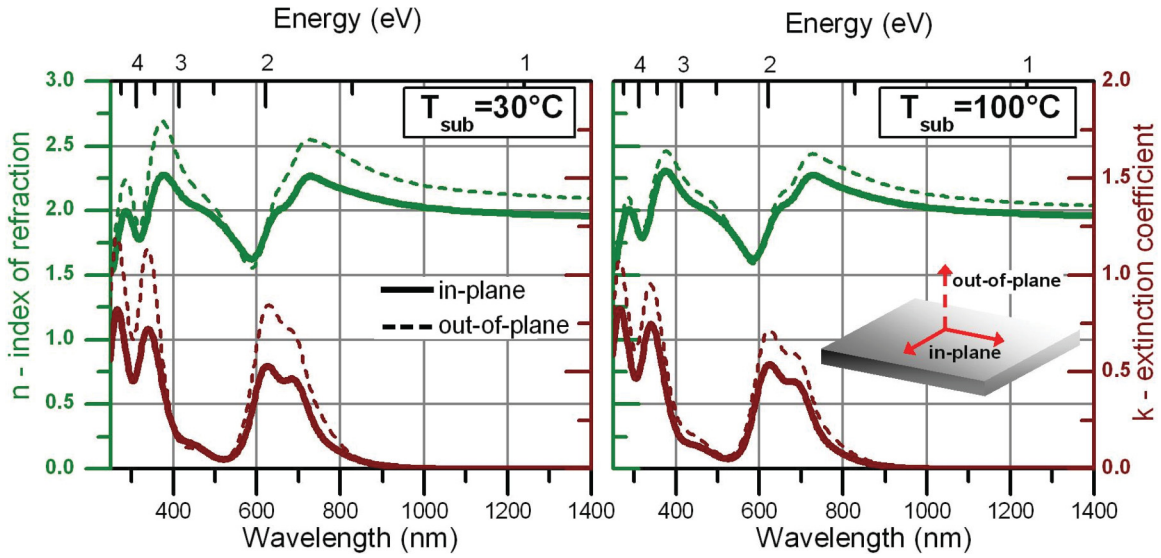

FIG. 5. (Color online) Anisotropic optical constants as determined by VASE measurements for 100-nm-thick ZnPc:C_{60} (1:1) blend layers deposited on SiO_2 substrates for substrate temperatures of 30 °C (left) and 100 °C (right). The dashed lines correspond to the out-of-plane and the solid line to the in-plane component of n (green) and k (dark red).

B. Mobility measurements

Bottom-contact organic field effect transistors are characterized in order to study how the morphological modification within the blend layers influences the electronic properties. Therefore 40-nm ZnPc:C_{60} (1:1) blends are deposited at different substrate temperatures of 30, 100, and 140 °C on SiO_2 substrate are characterized. For comparison, OFETs with 30-nm thick pristine ZnPc and C_{60} layers on unheated SiO_2 substrates are measured. Transistor geometry and sample preparation are given elsewhere.[30] A crucial point of OFET geometry is the fact that the charge carrier transport between source and drain takes place within the first nanometer of the ZnPc:C_{60} blend on the SiO_2-surface. Hence it is possible that the electron and hole mobility evaluated from the saturation regime of the OFET characteristics is not representative for the complete blend layer. However, different channel lengths are measured and no dependence is observed. In Fig. 6, the evaluated average hole and electron mobility values for each blend layer are shown. The hole mobility of the blend is constant at about 1×10^{-4} cm^2/Vs, independent of substrate temperatures. GIXRD measurements show, that the crystallinity of ZnPc stays unchanged for different T_{sub} (see Fig. 2). Considering that hole transport occurs within the ZnPc domains, the constant hole mobility correlates very well with the result of unchanged crystallinity. The hole mobility for the pristine ZnPc film is found to be 1.9×10^{-3} cm^2/Vs, more than one order of magnitude higher compared to the ZnPc:C_{60} blend.

Regarding the increase in crystallinity of C_{60} for substrate heated ZnPc:C_{60} blends (see Fig. 2) and that the mobility is known to be enhanced for crystalline organic material, as found by Karl *et al.*,[31] we would expect an increase in electron mobility for higher T_{sub}. However, the determined electron mobility shows a different trend and decreases from 5.4×10^{-2} cm^2/Vs for unheated blend layers to 0.2×10^{-2} cm^2/Vs for $T_{sub} = 140$ °C, as depicted in Fig. 6. As comparison the electron mobility for pristine C_{60} is found to be 2×10^{-1} cm^2/Vs.

When interpreting these data, it is important to consider that the determined mobility depends significantly on the channel morphology of the organic transistor. More specifically the calculated mobility is directly proportional to the current between source and drain, the channel length and is indirectly proportional to the channel width between the two gold contact.[32] For pristine organic layers, the geometrical influence is rather small, but for blend layers, the percolation paths of donor and acceptor domains form different channel geometries. The morphological results show that the phase separation between ZnPc and C_{60} is changing with substrate temperature. This implies that also the channel geometry, so

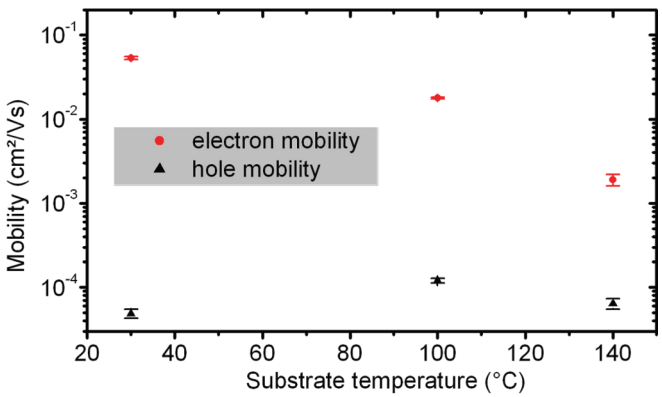

FIG. 6. (Color online) Substrate temperature dependency of electron (red/bright circles) and hole mobility (black squares) of ZnPc:C_{60} (1:1) blend layers measured by OFET. The 40-nm thick ZnPc:C_{60} blend layers are deposited on SiO_2 substrate with patterned Au contacts at different substrate temperatures of 25, 100, and 140 °C. The error bars represent the standard deviation of four mobility values evaluated from different OFETs on the same substrate with channel length of 10 and 20 μm.

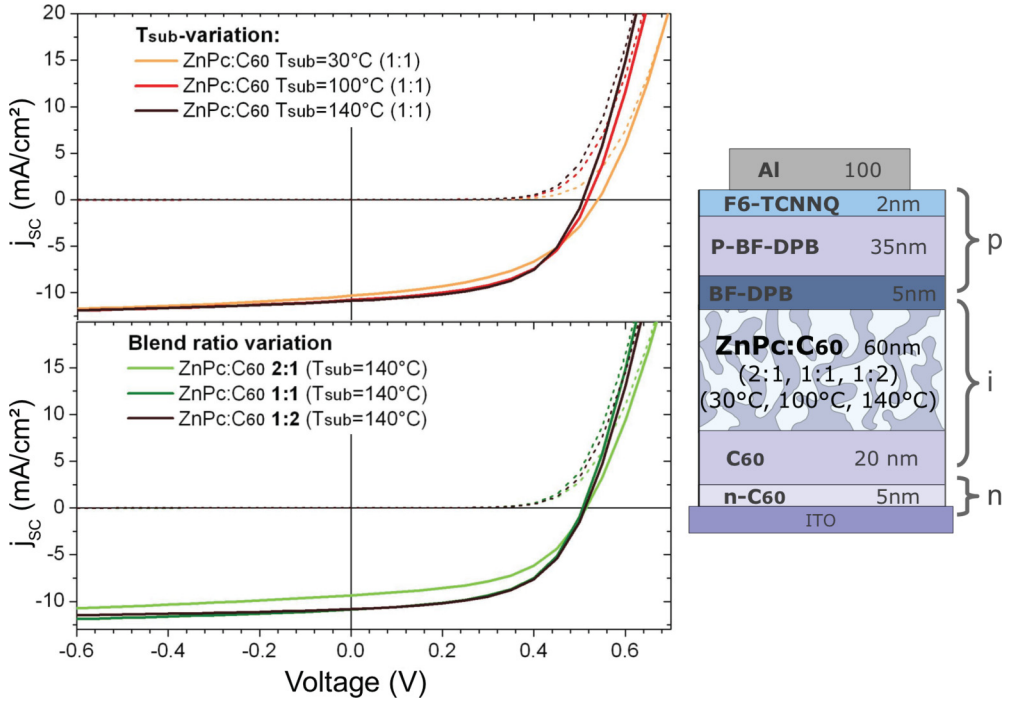

FIG. 7. (Color online) *j-V* curves and device stack of ZnPc:C_{60} bulk heterojunction solar cells using different blend ratios (lower part) and substrate temperature (upper part) during deposition. Solar cells stack: ITO (90 nm)/5-nm C_{60}:W2(hpp)4 (2 wt%)/20-nm C_{60}/60-nm ZnPc:C_{60} (1:1)/5-nm BF-DPB/35-nm BF-DPB:F6-TCNNQ (10 wt%)/2-nm F6-TCNNQ/100-nm Al.

length and width of paths for electrons and holes might be modified. So the observed change in electron mobility for different T_{sub} can also be caused by a formation of different percolation paths and not only by a change of the current flow. However, the change in electron mobility with T_{sub} is small and the large value of 5×10^{-2} cm^2/Vs reveal that percolation paths and phase separation are efficient, even for blend layers deposited on unheated substrates, confirming GIXRD results.

C. ZnPc:C_{60} bulk heterojunction solar cells

The most relevant application of ZnPc:C_{60} blend layers is as photoactive layer in bulk heterojunction organic solar cells. To prove how the observed morphological change influences the solar cell performance, nip solar cells with 60-nm-thick ZnPc:C_{60} (1:1) as absorber layer are fabricated. Substrate temperature and blend ratio are varied in the same manner as for the morphological investigations (see Figs. 2 and 3). By using a custom-made single chamber vacuum system (K. J. Lesker, UK), we are able to process all solar cells presented here within one run. Hence the comparability between these solar cells is very high. The solar cell stack is presented in Fig. 7 and the substrate is heated only during the ZnPc:C_{60} blend layer deposition. All other layers are deposited at room temperature.

The *j-V* curves and solar cell characteristics are presented in Fig. 7 and Table II. When heating the substrate the fill factor (FF) of the solar cells increases from 48.1% for the unheated blend layer over 53.7% for $T_{sub} = 100\,^{\circ}C$ to 55.3% for $T_{sub} = 140\,^{\circ}C$. Due to the enhancement in FF also the solar cell power conversion efficiency is improved from 2.6% to 3.0%. We also vary the blend ratio of the ZnPc:C_{60} absorber layer for 140 °C heated substrates analogues to the morphological investigations. The FF and the short circuit

TABLE II. Overview about the morphological results of the ZnPc:C_{60} blend layers and solar cell parameters of *j-V* characteristics of the ZnPc:C_{60} bulk heterojunctions shown in Fig. 6. I_{eff} is the mismatch corrected intensity that is used to calculate the correct power conversion efficiency η^*.

	Solar cell parameters					
Blend layer structure	Voc (V)	jsc (mA/cm²)	FF (%)	η^* (%)	Ieff (mW/cm²)	Morphology (from GIXRD and AFM)
ZnPc:C_{60} 1:1, $T_{sub} = 30\,^{\circ}C$	0.54	10.3	48.1	2.6	103.0	ZnPc and C_{60} amorphous, but phase separated
ZnPc:C_{60} 1:1, $T_{sub} = 100\,^{\circ}C$	0.52	10.8	53.7	2.9	102.1	C_{60} nanocrystalline, ZnPc amorphous
ZnPc:C_{60} 1:1, $T_{sub} = 140\,^{\circ}C$	0.51	10.9	55.2	3.0	102.2	C_{60} nanocrystalline, ZnPc amorphous
ZnPc:C_{60} 1:2, $T_{sub} = 140\,^{\circ}C$	0.51	10.8	55.6	3.0	102.4	C_{60} nanocrystalline, ZnPc amorphous
ZnPc:C_{60} 2:1, $T_{sub} = 140\,^{\circ}C$	0.51	9.4	52.6	2.5	101.9	ZnPc and C_{60} amorphous, but phase separated

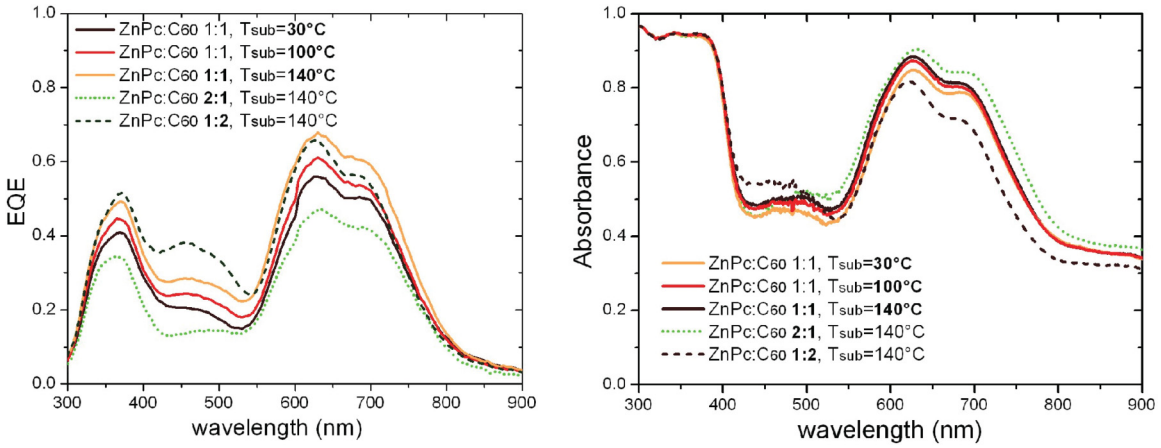

FIG. 8. (Color online) EQE (left) and absorbance (right) of the ZnPc:C_{60} bulk heterojunction solar cells shown in Fig. 6. The absorbance of the solar cells is measured in reflectance.

current density (jsc) of the amorphous (or nanocrystalline) 2:1 ZnPc:C_{60} blend are lower than for 1:1 and 1:2 blend layers, where C_{60} forms polycrystallites. Hence, also in this case, the fill factor is increased when C_{60} molecules form crystallites. Comparing jsc (see Table II) of the solar cells with the absorbance measurements shown in Fig. 8, it is evident that the change in jsc follows the same trend as absorption, except for 2:1 ZnPc:C_{60} at $T_{sub} = 140\,^{\circ}C$. Additionally, the absorbance measurements reveal an increased ZnPc absorption for the heated bulk heterojunction which can be directly attributed to the change in molecular orientation as found by VASE measurements (see Fig. 5). This indicates that the amount of excitons, which are dissociated, remains unchanged. Hence ZnPc and C_{60} domains are not so large that the exciton diffusion length is smaller than the domain size, inducing less exciton dissociation and therefore lower jsc. The small change in open circuit voltage (Voc) for different Tsub is discussed in Ref. 33. They state that the change in Voc might be due to a shift of the ZnPc HOMO level. However, the change in Voc is not very significant.

Both morphological and solar cell results indicate that blend layers with crystalline C_{60} domains lead to enhanced charge carrier transport. However, the increase in FF is not as significant as expected, indicating that the change in phase separation is not such significant. GIXRD pattern (see Figs. 2 and 3) confirm this, because for all investigated blend layers a certain phase separation is observed, reflected by the distinct C_{60} and ZnPc peak for all GIXRD scans. While ZnPc remains unchanged for all blend layers, only C_{60} changes to form nanocrystallites. An overview between morphological results and solar cell performance is given in Table II.

Additionally, external quantum efficiency (EQE) measurements are performed for the same solar cells. EQE describes the measured photocurrent of the complete solar cell per incoming photon flux varying the photon wavelengths. Because all solar cells show the same device geometry, except the discussed variations for the blend layer, changes in EQE are related to the blend layer morphology. Figure 8 shows a clear enhancement of EQE for all wavelength when heating the substrate of the solar cells while deposition of ZnPc:C_{60} (1:1). This illustrates that both charge carriers can be extracted more efficiently out of the blend layer to the electrode for stronger phase separation, correlated with higher T_{sub}. Furthermore, the small effect of slightly increased absorption of ZnPc within heated blend layers is amplifying this change in EQE. The most interesting point is presented by the low EQE of the 2:1 ZnPc:C_{60} layer, especially in the wavelength range of the Q absorption band (600–800 nm) of ZnPc. When using higher ZnPc content an increase in EQE for the ZnPc absorption region would be expected. This enhanced absorption for ZnPc for higher ZnPc contents of the ZnPc:C_{60} blend is shown in Fig. 8. However, the opposite is obtained, i.e., the EQE is even less as compared to the unheated ZnPc:C_{60} (1:1) blend. This directly indicates that percolation paths of the charge carriers are strongly disturbed. This observation is assigned to worse phase separation of ZnPc and C_{60} with inefficient percolation paths and it further supports the argument that a high C_{60} content is favorable for good phase separation and percolation paths.

Recently, Pfützner *et al.*[18] discussed the phase separation in ZnPc:C_{60} blend layers by the different interaction energies of the nearest neighbour molecules. They stated that the interaction energies between nearest neighbours are 0.87 eV for CuPc-CuPc, 1.5 eV for C_{60}-C_{60} and 0.44 eV for CuPc-C_{60}, respectively.[34–37] Pfützner *et al.*[18] assumed that the interaction energies of ZnPc-ZnPc and CuPc-CuPc are comparable due to their similar molecular structure. Examining only these values, the arrangement of C_{60} to C_{60} molecules is most preferred within blend layers and the total mixing of CuPc and C_{60} the most unfavored case. This directly implies the formation of separated ZnPc and C_{60} phases provided that the deposited molecules have enough kinetic energy to form C_{60} and ZnPc domains.

IV. CONCLUSION

We are able to influence the ZnPc:C_{60} blend layer morphology by using different substrate temperatures and different blend ratios for the blend layer preparation. An enhanced phase separation, resulting in improved percolation paths for electrons and holes, is achieved using high C_{60} contents within the blend (1:1, 1:2 by volume) and by heating the substrate during deposition. This improvement leads to an

enhancement in solar cell performance, i.e., an increase in fill factor from 48.1% to 55.6% and in power conversion efficiency from 2.5% to 3.0%. GIXRD measurements clearly reveal that unheated ZnPc:C_{60} blend layers are able to form separated ZnPc and C_{60} domains, providing a moderate fill factor of the unheated solar cell of 48%. However, when heating the substrate during deposition of the blend layer, C_{60} molecules are able to form crystallites due to an increased thermal excess energy by the heated substrate. In contrast, we do not observe a significant formation of ZnPc crystallites, although VASE measurements indicate a preferred upright standing orientation of ZnPc molecules within its domains. For 140 °C heated substrates, ZnPc:C_{60} blend layers are deposited using different blend ratios of 2:1, 1:1, and 1:2. The GIXRD measurement clearly indicates that also for high ZnPc content within the blend, ZnPc is not able to crystallize, even for elevated substrate temperatures of 140 °C. Surprisingly, C_{60} is not able to crystallize for 2:1 ZnPc:C_{60} blends for $T_{sub} = 140$ °C. EQE measurements of the corresponding solar cells show a significant decrease in EQE signal for these blend ratio compared to 1:1 especially for the absorption region of ZnPc. This clearly confirms that the phase separation becomes worse when using higher ZnPc amounts, indicating inefficient percolation paths.

All these findings clearly illustrate that the molecular arrangement of C_{60} is the driving force to enable efficient phase separation within ZnPc:C_{60} bulk heterojunction solar cells. The origin is presumably the spherical shape of C_{60}, which allows the formation of a dense, crystalline packing of C_{60} molecules more easily as for the planar ZnPc molecules. Due to the unique shape of C_{60} among all known organic semiconductors, it might play a key role for phase separation of organic blend layers in general. However, this behavior can differ when using other donor materials in combination with C_{60}. Hence this hypothesis will be proven by investigating different donor-C_{60} blend layer systems in near future.

ACKNOWLEDGMENTS

This work is financially supported by the Bundesministerium für Bildung und Forschung (BMBF) within the project 13N9872 and by the Free State of Saxony and the European Union via the European Regional Development Fund (ERDF) under SAB project number 71070.

*Corresponding author: christoph.schuenemann@iapp.de
†Current adress: University of California Santa Barbara, US.
‡Current adress: Novaled AG, 01307 Dresden, Germany.
§Corresponding author: karl.leo@iapp.de

[1] M. A. Green, K. Emery, Y. Hishikawa, W. Warta, and E. D. Dunlop, Progr. Photovoltaics **19**, 565 (2011).
[2] P. Würfel, CHIMIA Int. J. Chem. **61**, 770 (2007).
[3] C. W. Tang, Appl. Phys. Lett. **48**, 183 (1986).
[4] R. R. Lunt, N. C. Giebink, A. A. Belak, J. B. Benziger, and S. R. Forrest, J. Appl. Phys. **105**, 053711 (2009).
[5] B. Maennig *et al.*, Appl. Phys. A **79**, 1 (2004).
[6] P. Peumans, A. Yakimov, and S. R. Forrest, J. Appl. Phys. **93**, 3693 (2003).
[7] G. Yu, J. Hummelen, F. Wudl, and A. Heeger, Science **270**, 1789 (1995).
[8] M. Hiramoto, K. Suemori, and M. Yokoyama, Jpn. J. Appl. Phys. **41**, 2763 (2002).
[9] C. R. McNeill, J. J. M. Halls, R. Wilson, G. L. Whiting, S. Berkebile, M. G. Ramsey, R. H. Friend, and N. C. Greenham, Adv. Funct. Mater. **18**, 2309 (2008).
[10] P. Peumans, S. Uchida, and S. R. Forrest, Nature (London) **425**, 158 (2003).
[11] R. A. Marsh, C. Groves, and N. C. Greenham, J. Appl. Phys. **101**, 083509 (2007).
[12] P. K. Watkins, A. B. Walker, and G. L. B. Verschoor, Nano Lett. **5**, 1814 (2005).
[13] F. Yang and S. R. Forrest, ACS Nano **2**, 1022 (2008).
[14] B. P. Rand, J. Xue, S. Uchida, and S. R. Forrest, J. Appl. Phys. **98**, 124902 (2005).
[15] Z. R. Hong, B. Maennig, R. Lessmann, M. Pfeiffer, K. Leo, and P. Simon, Appl. Phys. Lett. **90**, 203505 (2007).
[16] X. Yang, J. Loos, S. C. Veenstra, W. J. H. Verhees, M. M. Wienk, J. M. Kroon, M. A. J. Michels, and R. A. J. Jansen, Nano Lett. **5**, 579 (2005).
[17] B. Servet, G. Horowitz, S. Ries, O. Lagorsse, P. Alnot, A. Yassar, F. Deloffre, P. Srivastava, and R. Hajlaoui, Chem. Mater. **6**, 1809 (1994).
[18] S. Pfuetzner, J. Meiss, A. Petrich, M. Riede, and K. Leo, Appl. Phys. Lett. **94**, 253303 (2009).
[19] W. Tress, K. Leo, and M. Riede, Sol. Energ. Mat. Sol. C. **95**, 2981 (2011).
[20] F. Padinger, R. S. Rittberger, and N. S. Sariciftci, Adv. Funct. Mater. **13**, 85 (2003).
[21] C. Schünemann, C. Elschner, A. A. Levin, M. Levichkova, K. Leo, and M. Riede, Thin Solid Films **519**, 3939 (2011).
[22] C. Elschner, A. A. Levin, L. Wilde, J. Grenzer, C. Schroer, K. Leo, and M. Riede, J. Appl. Crystallogr. **44**, 983 (2011).
[23] D. Yokoyama, A. Sakaguchi, M. Suzuki, and C. Adachi, Org. Electronics **10**, 127 (2009).
[24] D. Wynands, M. Erber, R. Rentenberger, M. Levichkova, K. Walzer, K.-J. Eichhorn, and M. Stamm, Org. Electronics **13**, 885 (2012).
[25] A. Opitz, M. Bronner, and W. Brütting, J. Appl. Phys. **101**, 063709 (2007).
[26] K. Suemori, T. Miyata, M. Yokoyama, and M. Hiramoto, Appl. Phys. Lett. **86**, 063509 (2005).
[27] P. Simon, B. Maennig, and H. Lichte, Adv. Funct. Mater. **14**, 669 (2004).
[28] B. Maennig, M. Pfeiffer, A. Nollau, X. Zhou, K. Leo, and P. Simon, Phys. Rev. B **64**, 195208 (2001).
[29] A. Henriksson and M. Sundbom, Theoretica Chimica Acta **27**, 213 (1972).
[30] M. S. Wrackmeyer, M. Hein, A. Petrich, J. Meiss, M. Hummert, M. K. Riede, and K. Leo, Sol. Energ. Mater. Sol. C. **95**, 3171 (2011).
[31] N. Karl, Synth. Met. **133–134**, 649 (2003).
[32] G. Horowitz, Adv. Mater. **10**, 365 (1998).
[33] W. Tress, S. Pfuetzner, K. Leo, and M. Riede, J.Photon. Energ. **1**, 011114 (2011).

[34]V. P. Antropov, O. Gunnarsson, and O. Jepsen, Phys. Rev. B **46**, 13647 (1992).
[35]D. J. Liu, R. L. Blumberg Selinger, and J. D. Weeks, J. Chem. Phys. **105**, 4751 (1996).
[36]M. Fendrich, T. Wagner, M. Stöhr, and R. Möller, Phys. Rev. B **73**, 115433 (2006).
[37]R. W. Lof, M. A. Veenendaal, B. Koopmans, H. T. Jonkman, and G. A. Sawatzky, Phys. Rev. Lett. **68**, 3924 (1992).
[38]T. Menke, D. Ray, J. Meiss, K. Leo, and M. Riede, Appl. Phys. Lett. **100**, 093304 (2012).
[39]R. M. A. Azzam and N. M. Bashara, *Ellipsometry and Polarized Light* (North-Holland, 1987).
[40]H. Fujiwara, *Spectroscopic Ellipsometry: Principles and Applications* (Wiley, 2007).
[41]J. Hilfiker, N. Singh, T. Tiwald, D. Convey, S. Smith, J. Baker, and H. Tompkins, Thin Solid Films **516**, 7979 (2008).
[42]G. A. Kumar, J. Thomas, N. George, N. V. Unnikrishnan, P. Radhakrishnan, V. P. N. Nampoori, and C. P. Vallabhan, J. Mater. Sci. **35**, 2539 (2000).
[43]F. Yan, Y. N. Wang, and J. S. Liu, Europhys. Lett. **48**, 662 (1999).